Appl Phys B (2009) 96: 301–308
DOI 10.1007/s00340-009-3594-9

Applied Physics B
Lasers and Optics

Concept of area scintillation

H.T. Eyyuboğlu

Received: 13 February 2009 / Published online: 6 June 2009

Abstract Stemming from the results of our earlier investigations, the concept of area scintillation is introduced, which takes into account the intensity distribution over the receiver plane. In this context, the area scintillation of fundamental Gaussian and annular beams is formulated, numerically evaluated and graphically illustrated. From the comparison, it is seen that, under the same source power conditions, annular Gaussian beams provide much less scintillations than the fundamental Gaussian beams at small source size. At large source sizes and at shorter propagation distances, annular beams are still favorable, but, as the propagation range is extended, the reverse becomes true. A review of previous findings leading up to the newly introduced concept is also presented.

PACS 29.27.Fh · 41.85.Ew · 42.60.Jf · 42.68.Bz · 87.56.N-

1 Introduction

Scintillations are basically the intensity fluctuations in the received optical wave due to refractive index variations of the propagation medium. Their foundations are well established by the pioneers, Tatarskii, Ishimaru, Andrews, and Phillips [1–3]. Over the last years, we have attempted to examine the scintillation properties of beams other than the fundamental Gaussian beam, including coherent and incoherent versions of annular, cosh and cos beams and their coherent higher order counterparts, elliptical Gaussian beam, coherent, partially coherent and incoherent versions of flat-topped beams, dark hollow beams, Bessel beams and partially coherent multi Gaussian beams incorporating annular and flat-topped beams [4–17]. The findings from these studies may be summarized as follows:

- Inevitably, scintillation will grow with rises in propagation lengths [4–17].
- Higher wavelengths will cause less scintillations, except for the incoherent flat topped limit [4, 5, 7, 12, 14], where initially a rise is observed [7, 8].
- The scintillation behavior of other beams against source size is more or less similar to that of the fundamental Gaussian beam, except again for the incoherent flat topped limit [4–8, 10, 11, 13, 16, 17], where scintillation steadily falls against the growing source sizes [7, 8], and no plane wave limit is achievable in the case of annular beam [5].
- Scintillation generally acts in an opposite manner to intensity, in particular, toward the beam edges [6, 12, 13, 15].
- Focusing aids to reduce scintillation [5, 6].
- For multi-beam configurations, rising number of beams generally results in lower scintillation at limits of complete source coherence and incoherence [4, 7, 11, 12, 14], whereas in the partially coherent situation, higher number of beams gives rise to increased scintillation [17].
- Scintillation generally decreases as the source coherence is lowered [17].
- Little variations are experienced with changes in inner and outer scale of turbulence [6, 12, 14, 16].
- Under Rytov approximation, scintillation becomes linearly proportional to refractive index structure constant [4–6, 9–16], but, in the extended Huygens–Fresnel prin-

H.T. Eyyuboğlu (✉)
Electronic and Communication Engineering Department,
Çankaya University, Öğretmenler Cad. No. 14 Yüzüncüyıl,
06530 Balgat, Ankara, Turkey
e-mail: h.eyyuboglu@cankaya.edu.tr
Fax: +90-312-2848043

ciple, the variation of scintillation with refractive index structure constant follows a non-linear pattern [8, 17].
- Built on the perturbations of the free space expressions, Rytov approximation fails to account for points of the beam profile, where there is zero free space intensity [15, 16].

It is to be emphasized, however, that in all above treatments scintillation is formulated and illustrated for a single coordinate location on the receiver plane under the name of scintillation index. Obviously, such a quantity does not reflect, in a healthy manner, the overall status in the free space optical receivers since practical receivers capture the incident beam over an area rather than a single point.

Bearing this operational reality in mind, this work aims to introduce the concept of area scintillation. For this purpose, as detailed in the next section, we inversely scale the scintillation index with respect to the intensity of that particular receiver location, whilst integrating over the entire receiver capture area. We further bring up a new principle in the present analysis, which is comparing scintillation characteristics of beams that possess the same source power. This is in contrast to the approach taken in the earlier studies where comparisons were made on the basis of equating a single source parameter, such as source size, displacement parameter, number of beams in the beam composition, etc. As noted in a recent study [13], the setting of source parameters to be equal individually will create different power levels for different beam types. Thus this kind of comparison may result in misleading physical interpretations. In this sense, assessing the scintillation performance of beams from the same source power perspective is both physically more meaningful and also gives the chance of adjusting the several parameters in hand to perhaps lower scintillation.

2 Formulation of area scintillation

The source field of interest, $u_s(r_s, \phi_s)$, is supplied by the following expression

$$u_s(r_s, \phi_s) = \sum_{\ell=1}^{N} A_\ell \exp\left(-\alpha_\ell k r_s^2\right) \tag{1}$$

where r_s and ϕ_s are the radial coordinates of the source plane, via the index ℓ, N governs the number of components that will be involved in the summation, A_ℓ is the amplitude factor, $k = 2\pi/\lambda$ is the wave number, with λ being the wavelength, $\alpha_\ell = 1/(k\alpha_{s\ell}^2) + j/F_\ell$ with $\alpha_{s\ell}$ being the source size, F_ℓ the focusing parameter, and $j = \sqrt{-1}$. The fundamental Gaussian beam consists of a single component; hence, $N = 1$. Annular beam, on the other hand, has two components named primary and secondary; hence, $N = 2$. In both cases, the beams are circularly symmetric; nevertheless, we will carry through the angular variable ϕ_s for physical consistency.

The total source power generated by the beam given in (1) is

$$\begin{aligned} P_s &= \int_0^\infty \int_0^{2\pi} dr_s\, d\phi_s\, r_s u_s(r_s, \phi_s) u_s^*(r_s, \phi_s) \\ &= \int_0^\infty \int_0^{2\pi} dr_s\, d\phi_s\, r_s I_s(r_s, \phi_s) \end{aligned} \tag{2}$$

where * indicates the complex conjugate and $I_s(r_s, \phi_s)$ corresponds to the intensity in $u_s(r_s, \phi_s)$. Upon substituting from (1) for $u_s(r_s, \phi_s)$, (2) will become

$$P_s = \pi \sum_{\ell_1=1}^{N} \sum_{\ell_2=1}^{N} A_{\ell_1} A_{\ell_2}^* \frac{\alpha_{s\ell_1}^2 \alpha_{s\ell_2}^2}{\alpha_{s\ell_1}^2 + \alpha_{s\ell_2}^2} \tag{3}$$

By demanding that the fundamental Gaussian and annular beams deliver the same source power, it is possible to compile form (3) a set of values for the amplitude factors and the source sizes. A range of selected parameters satisfying this condition is plotted in Fig. 1. Here, for simplicity, we have normalized the amplitude factors with respect to the amplitude factor of the primary component of the annular beam. This way, in Fig. 1, for the case of Gaussian beam, A_1 is read from the horizontal axis and labeled as A_G, while A_2 in the legend boxes of Fig. 1 refers to the amplitude factor of the secondary component of the annular beam, read from the vertical axis. Similarly, the source sizes of the fundamental Gaussian beam α_{sG} and the secondary component of the annular beam α_{s2} are scaled with respect to source size of the primary component of the annular beam α_{s1} through the following ratios

$$\varepsilon_G = \frac{\alpha_{sG}}{\alpha_{s1}}, \qquad \varepsilon_a = \frac{\alpha_{s2}}{\alpha_{s1}} \tag{4}$$

Using the von Karman spectrum, the scintillation index $m^2(r_r, \phi_r)$ for a single location of the receiver plane, that is, L distance apart from the source plane, is given in (9) of [6]. After adapting it for the beam type supplied in (1) and subsequently making the appropriate rearrangements, the scintillation index will read

$$m^2(r_r, \phi_r) = 1.3028 C_n^2 k^2 \,\mathrm{Re}\left[\frac{1}{D_a(r_r, \phi_r)} \sum_{\ell_1=1}^{N} \sum_{\ell_2=1}^{N} \sum_{m=0}^{\infty} \left(\frac{2\pi}{L_0}\right)^{2m-\frac{5}{3}} \frac{A_{\ell_1} A_{\ell_2}^* (\alpha_{\ell_1} + \alpha_{\ell_2}^*)^{2m} r_r^{2m}}{m![1 + 2j(\alpha_{\ell_1} - \alpha_{\ell_2}^*)L + 4\alpha_{\ell_1}\alpha_{\ell_2}^* L]^{2m+1}} \right.$$

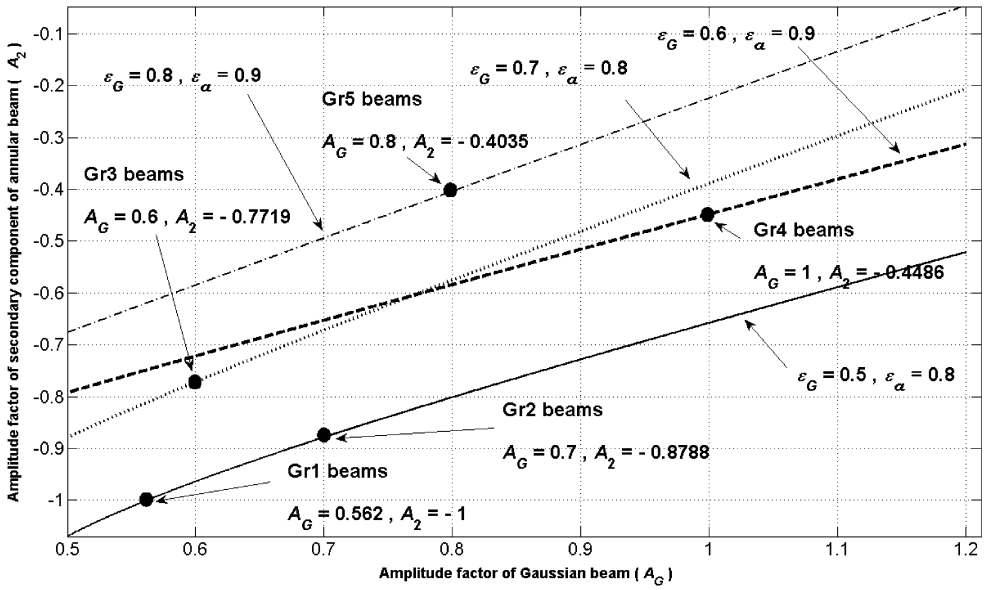

Fig. 1 Curves of same source power beams

$$\times \exp\left[-\frac{(\alpha_{\ell_1}+\alpha_{\ell_2}^*)kr_r^2}{1+2j(\alpha_{\ell_1}-\alpha_{\ell_2}^*)L+4\alpha_{\ell_1}\alpha_{\ell_2}^*L^2}\right]\int_0^L d\eta\,(L-\eta)^{2m}$$

$$\times U\left(m+1,m+1/6,\left\{\frac{(L-\eta)^2(\alpha_{\ell_1}+\alpha_{\ell_2}^*)}{[1+2j(\alpha_{\ell_1}-\alpha_{\ell_2}^*)L+4\alpha_{\ell_1}\alpha_{\ell_2}^*L^2]k}+0.0285l_0^2\right\}\left(\frac{2\pi}{L_0}\right)^2\right)$$

$$-\frac{1}{D_c(r_r,\phi_r)}\sum_{\ell_1=1}^{N}\sum_{\ell_2=1}^{N}\sum_{m=0}^{\infty}\left(\frac{2\pi}{L_0}\right)^{2m-\frac{5}{3}}\frac{A_{\ell_1}A_{\ell_2}(\alpha_{\ell_1}-\alpha_{\ell_2})^{2m}r_r^{2m}}{m![1+2j(\alpha_{\ell_1}+\alpha_{\ell_2})L-4\alpha_{\ell_1}\alpha_{\ell_2}L^2]^{2m+1}}$$

$$\times \exp\left[-\frac{(\alpha_{\ell_1}+\alpha_{\ell_2}+4j\alpha_{\ell_1}\alpha_{\ell_2}L)kr_r^2}{1+2j(\alpha_{\ell_1}+\alpha_{\ell_2})L-4\alpha_{\ell_1}\alpha_{\ell_2}L^2}\right]\int_0^L d\eta\,(L-\eta)^{2m}$$

$$\times U\left(m+1,m+1/6,\left\{\frac{(L-\eta)[j-(L-\eta)(\alpha_{\ell_1}+\alpha_{\ell_2})-4j\alpha_{\ell_1}\alpha_{\ell_2}\eta L]}{[1+2j(\alpha_{\ell_1}+\alpha_{\ell_2})L-4\alpha_{\ell_1}\alpha_{\ell_2}L^2]k}+0.0285l_0^2\right\}\left(\frac{2\pi}{L_0}\right)^2\right)\Bigg] \tag{5}$$

where the functions $D_a(r_r,\phi_r)$ and $D_c(r_r,\phi_r)$ are defined as follows

$$D_a(r_r,\phi_r)=\sum_{\ell_1=1}^{N}\sum_{\ell_2=1}^{N}\frac{A_{\ell_1}A_{\ell_2}^*}{1+2j(\alpha_{\ell_1}-\alpha_{\ell_2}^*)L+4\alpha_{\ell_1}\alpha_{\ell_2}^*L^2}\times\exp\left[-\frac{(\alpha_{\ell_1}+\alpha_{\ell_2}^*)kr_r^2}{1+2j(\alpha_{\ell_1}-\alpha_{\ell_2}^*)L+4\alpha_{\ell_1}\alpha_{\ell_2}^*L^2}\right] \tag{6a}$$

$$D_c(r_r,\phi_r)=\sum_{\ell_1=1}^{N}\sum_{\ell_2=1}^{N}\frac{A_{\ell_1}A_{\ell_2}}{1+2j(\alpha_{\ell_1}+\alpha_{\ell_2})L-4\alpha_{\ell_1}\alpha_{\ell_2}L^2}\times\exp\left[-\frac{(\alpha_{\ell_1}+\alpha_{\ell_2}+4j\alpha_{\ell_1}\alpha_{\ell_2}L)kr_r^2}{1+2j(\alpha_{\ell_1}+\alpha_{\ell_2})L-4\alpha_{\ell_1}\alpha_{\ell_2}L^2}\right] \tag{6b}$$

In (5) and (6), r_r and ϕ_r are the receiver plane radial coordinates, C_n^2 is refractive index structure constant, Re refers to the real part of the enclosed expression, ! means the factorial notation, $U(\,)$ is the confluent hypergeometric function of the second kind, l_0 and L_0 respectively stand for the inner and outer scales of turbulence. Note that the bracketing error found in the final argument of $U(\,)$ in the referenced manuscript [6] is corrected in (5).

Considering the already stated inverse relationship between the scintillation index and the intensity levels, we propose the area scintillation to be in the form of

$$m_A^2=\int_0^{r_0}\int_0^{2\pi}dr_r\,d\phi_r\,r_r\frac{m^2(r_r,\phi_r)}{I_r(r_r,\phi_r)} \tag{7}$$

where r_0 corresponds to the radius of (circular) receiver area, otherwise known as receiver aperture radius, and

$I_r(r_r, \phi_r)$ is the intensity distribution over the same area. Including the effects of turbulence, the intensity can be retrieved from (6) of [18] after rearranging it for the beam type of (1). This way $I_r(r_r, \phi_r)$ will turn out to be

$$I_r(r_r,\phi_r)=\sum_{\ell_1=1}^{N}\sum_{\ell_2=1}^{N}\frac{A_{\ell_1}A_{\ell_2}^{*}k\rho_0^2}{k\rho_0^2+2j(\alpha_{\ell_1}-\alpha_{\ell_2}^{*})k\rho_0^2L+4(\alpha_{\ell_1}+\alpha_{\ell_2}^{*})L^2+4\alpha_{\ell_1}\alpha_{\ell_2}^{*}k\rho_0^2L^2}$$
$$\times\exp\left[-\frac{(\alpha_{\ell_1}+\alpha_{\ell_2}^{*})k^2\rho_0^2r_r^2}{k\rho_0^2+2j(\alpha_{\ell_1}-\alpha_{\ell_2}^{*})k\rho_0^2L+4(\alpha_{\ell_1}+\alpha_{\ell_2}^{*})L^2+4\alpha_{\ell_1}\alpha_{\ell_2}^{*}k\rho_0^2L^2}\right] \tag{8}$$

where $\rho_0=(0.546C_n^2k^2L)^{-3/5}$ is called the coherence length of the spherical wave. By insertion of (5), (6) and (8) into (7), area scintillation m_A^2 can be evaluated numerically.

3 Results and discussions

In this section, we calculate area scintillation for the fundamental Gaussian and annular beams, commenting on the results. It should be noted that, although according to (5) and (7), computation of m_A^2 entails a triple integral, the integration over ϕ_r simply produces 2π since our beams contain no angular dependence. This way the evaluation of m_A^2 in (7) reduces to a double integral, and can thus be performed with the previously utilized efficient routine [19].

To ensure that the same source power condition is fulfilled, we choose the source parameters for the two beams from the curves of Fig. 1. To have a good range of samples, we choose five groups of beams from Fig. 1, naming them sequentially as Gr1, Gr2, Gr3, Gr4, and Gr5 beams. The parameters of selected Gaussian and annular beams are also listed in Table 1, where the absolute power P_s obtained from (3) is stated (in watts) in the last column, assuming the amplitude factors are measured in volts. Note that, since ε_G and ε_a merely express the ratios of the source sizes for Gaussian and annular beams, the absolute values of source sizes are determined after setting α_{s1} which is the source size of the primary component of the annular beam. In this study, we use two settings: $\alpha_{s1}=1$ cm and 5 cm. Figure 2 offers the intensity profiles of the selected groups of beams cut along any circumferential position ϕ_s. As seen form Fig. 2, in Gr1, Gr2 and Gr3, the annular beams exhibit the conventional well type of structure, whereas in Gr4 and Gr5, the profiles of annular beams are nearly indistinguishable from the Gaussian profiles. Figure 2 also demonstrates that in this set of same source power beams, annular beams will always have a larger source beam size (whose definition is given in [19]) than fundamental Gaussian beams.

By setting $\alpha_{s1}=1$ cm, Fig. 3 shows the variation of area scintillation m_A^2 for Gr1 and Gr2 beams, where the radius of receiver area $r_0=1$ cm is kept the same all along the propagation range considered. As expected, the area scintillation increases with rising propagation distance. But these rises seem to be more substantial for Gaussian beams. The same trend is observed in Fig. 4 that displays the variation of area scintillation m_A^2 for Gr3, Gr4 and Gr5 beams.

Table 1 Parameters of selected same source power beams

	Beam type	ε_G or ε_a	A_1 or A_G for Gaussian beam	A_2	P_s (in watt) for $\alpha_{s1}=1$ cm	P_s (in watt) for $\alpha_{s1}=5$ cm
Gr1	Gaussian	0.5	0.562	0	1.2413×10^{-5}	3.1033×10^{-4}
	Annular	0.8	1	−1		
Gr2	Gaussian	0.5	0.7	0	1.9239×10^{-5}	4.8098×10^{-5}
	Annular	0.8	1	−0.8788		
Gr3	Gaussian	0.7	0.6	0	2.7711×10^{-5}	6.9278×10^{-4}
	Annular	0.8	1	−0.7719		
Gr4	Gaussian	0.6	1	0	5.6547×10^{-5}	1.4137×10^{-3}
	Annular	0.9	1	−0.4486		
Gr5	Gaussian	0.8	0.8	0	6.4338×10^{-5}	1.6085×10^{-3}
	Annular	0.9	1	−0.4035		

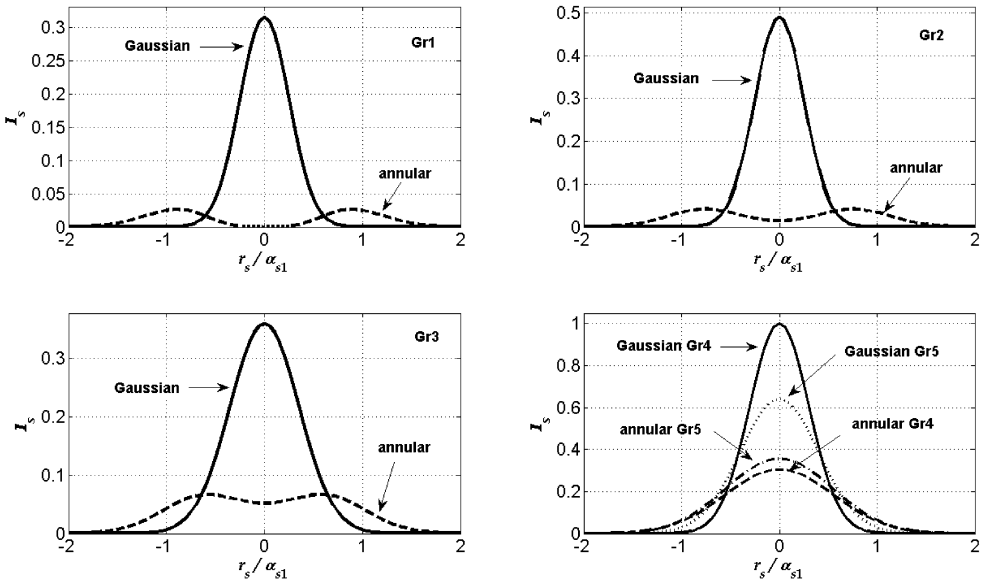

Fig. 2 Intensity profiles of same source power beams

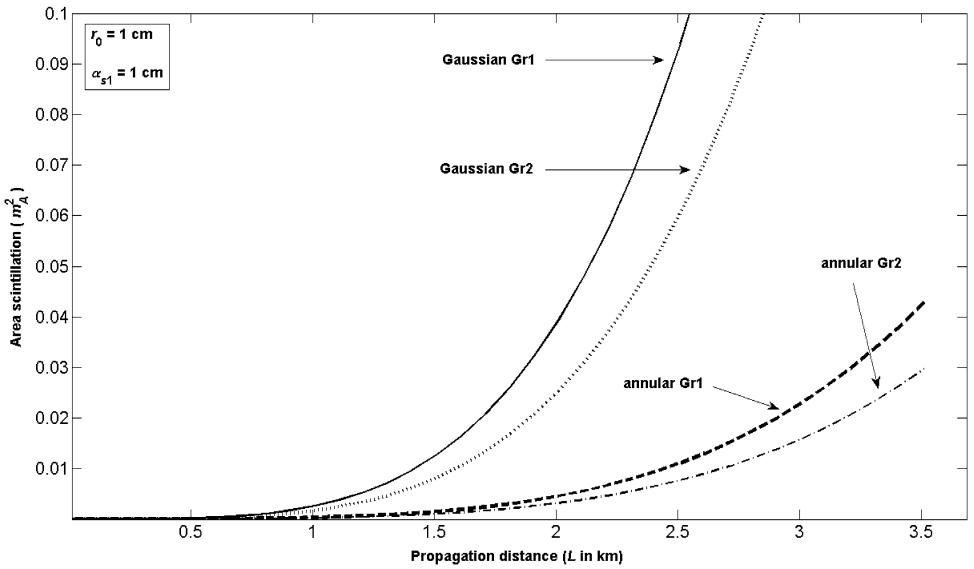

Fig. 3 Variation of area scintillation against propagation distance for Gr1 and Gr2 beams at $\alpha_{s1} = 1$ cm

The above situation changes, however, when we switch to $\alpha_{s1} = 5$ cm as illustrated in Fig. 5 for Gr1 and Gr2 beams, where r_0 is also raised to 5 cm. In comparison to Fig. 3, two main differences can be identified in Fig. 5. The first one is that, at short propagation distances, the area scintillation of Gaussian beams possesses a bump; the second is that, at long propagation distances, the area scintillations of Gaussian beams fall below those of annular beams. The first effect is due to the fact that large source sized beams face less diffraction than those with smaller source sizes [19]. At distances extremely close to the source plane, the cumulative amount of area scintillations is much less; hence, for both Figs. 3 and 5, area scintillations initially start from zero. But as we go along the propagation axis, the Gaussian beams scaled to $\alpha_{s1} = 5$ cm, i.e., those Gaussian beams of Fig. 5, suffer less diffraction than those Gaussian beams scaled to $\alpha_{s1} = 1$ cm, i.e., the Gaussian beams of Fig. 3. In this manner, for a larger source sized Gaussian beam expanding less upon propagation, at a receiver capture radius of $r_0 = 5$ cm, the edges of the beam remain longer at intensity levels well below the peak value. This phenomenon causes the area scintillation to grow excessively, giving rise to the bumps encountered in Fig. 5. But this effect disappears as the propagation distance is increased, with diffraction causing the intensity levels at the beam edges to rise. On the other hand, in the case of beams scaled to $\alpha_{s1} = 1$ cm, diffraction begins at earlier propagation distances. Thus the edges of the beams attain such intensity levels much sooner; therefore, these bumpy appearances of Fig. 5 cannot be observed in Fig. 3. Moreover, as seen from Fig. 2, under the condition of same source power, the source beam sizes of annular beams are always larger than those of Gaussian beams. This fact

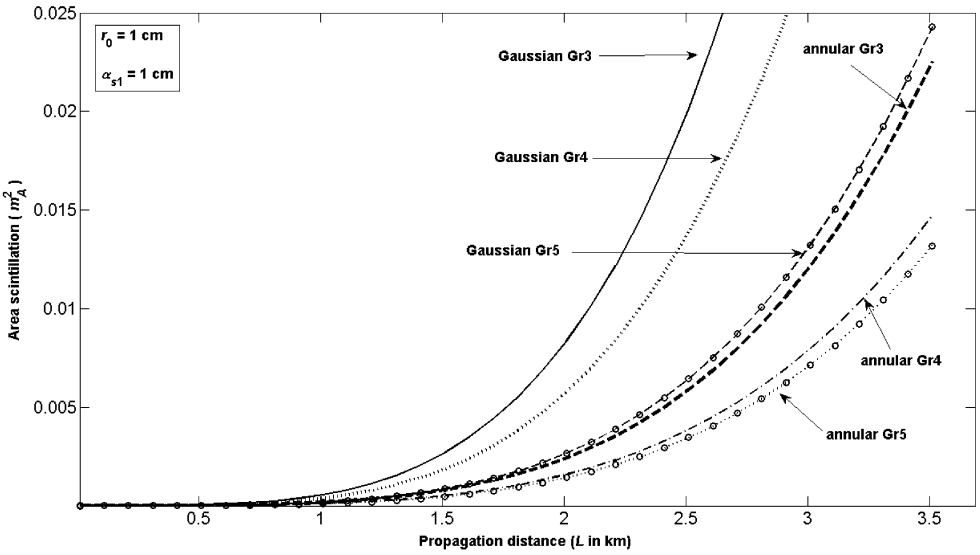

Fig. 4 Variation of area scintillation against propagation distance for Gr3, Gr4 and Gr5 beams at $\alpha_{s1} = 1$ cm

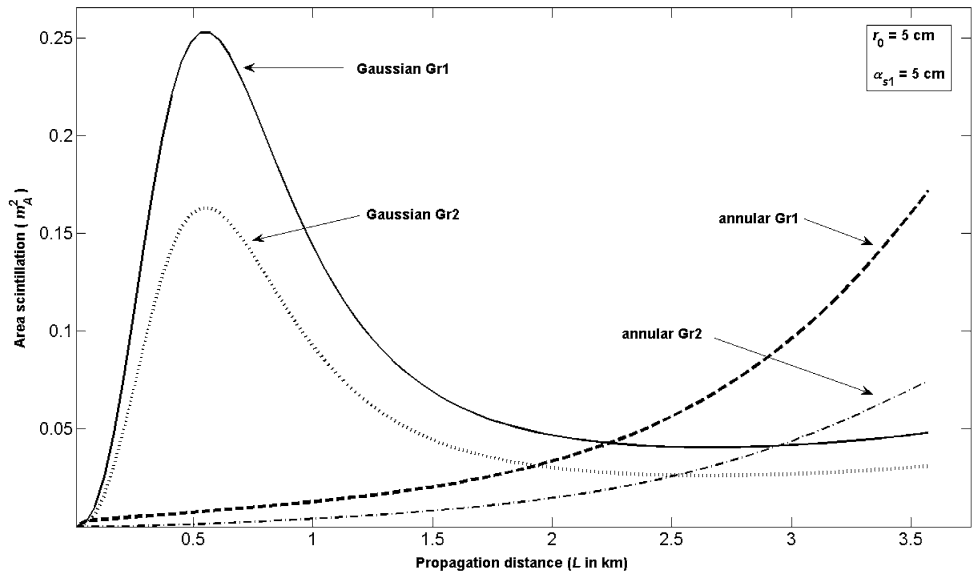

Fig. 5 Variation of area scintillation against propagation distance for Gr1 and Gr2 beams at $\alpha_{s1} = 5$ cm

prevents the occurrence of bumps for annular beams at a setting of $r_0 = 5$ cm. Finally, the differences found between Fig. 3 and Fig. 5, i.e., at small source sizes, annular beams being more advantageous than Gaussian beams and the reverse happening at large source sizes, seem to be in line with the findings of [5], where on-axis, i.e., single point scintillation, is examined.

Figure 6 shows that the area scintillation behavior of Fig. 5 continues when Gr3, Gr4 and Gr5 beams are selected. But in this case, the bumps become smoother, extending into longer propagation distances.

For the beams of Gr1, Gr2, Gr3, Gr4, and Gr5, we plot in Fig. 7 the power captured by the receiver for the two aperture openings of $r_0 = 1$ cm and 5 cm, where it is seen that, apart from the distances extremely close to the source plane, more power is captured for annular beams when $r_0 = 1$ cm, while the reverse holds at $r_0 = 5$ cm. For this plot, $P_r(r_0)$ is calculated from the following integral.

$$P_r(r_0) = 2\pi \int_0^{r_0} dr_r \, I_r(r_r, \phi_r) r_r = \pi \sum_{\ell_1=1}^{N} \sum_{\ell_2=1}^{N} A_{\ell_1} A_{\ell_2}^* \frac{\alpha_{s\ell_1}^2 \alpha_{s\ell_2}^2}{\alpha_{s\ell_1}^2 + \alpha_{s\ell_2}^2}$$
$$\times \left\{ 1 - \exp\left[- \frac{(\alpha_{\ell_1} + \alpha_{\ell_2}^*) k \rho_0^2 r_0^2}{k\rho_0^2 + 2j(\alpha_{\ell_1} - \alpha_{\ell_2}^*) k \rho_0^2 L + 4(\alpha_{\ell_1} + \alpha_{\ell_2}^*) L^2 + 4\alpha_{\ell_1} \alpha_{\ell_2}^* k \rho_0^2 L^2} \right] \right\} \tag{9}$$

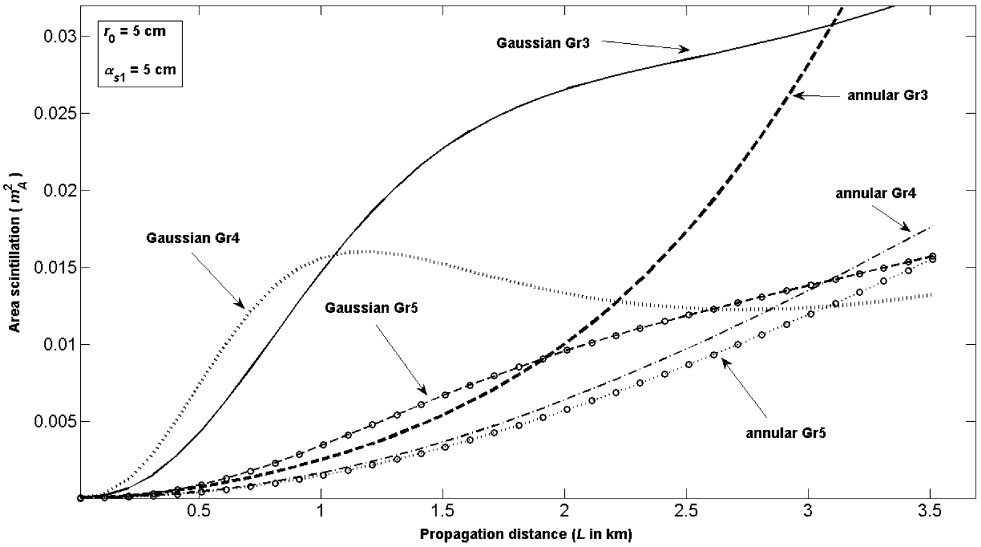

Fig. 6 Variation of area scintillation against propagation distance for Gr3, Gr4 and Gr5 beams at $\alpha_{s1} = 5$ cm

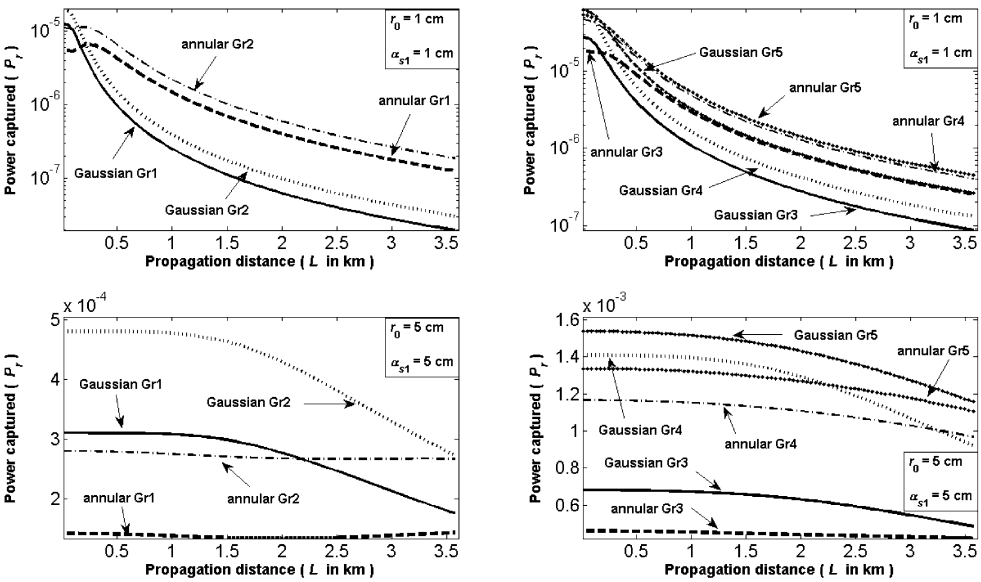

Fig. 7 Power captured by Gr1, Gr2, Gr3, Gr4, and Gr5 beams for $r_0 = 1$ and 5 cm

where $I_r(r_r, \phi_r)$ is taken from (8).

Finally, we explore in Fig. 8 the dependence of area scintillation on the receiver aperture radius r_0. From the respective beams present in the subplots of Fig. 8, it is seen that, at $\alpha_{s1} = 1$ cm, the ordering of beams is similar to the variations against propagation lengths found in Figs. 3 and 4. For $\alpha_{s1} = 5$ cm, however, Gaussian beams have less area scintillations at small aperture sizes, while this changes in favor of annular beams as aperture becomes larger. Additionally, the trends of the curves in Fig. 8 indicate that more scintillations are bound to occur as the receiver capture area is widened.

4 Conclusion

In this work, we have presented the concept of area scintillation and analyzed the fundamental Gaussian and annular beams in this respect. Our comparisons indicate that under the conditions of same source power, at smaller source sizes, with the receiver aperture radius set to the source size of the primary component of the annular beam, Gaussian beams generate more area scintillations than annular beams. On the other hand, when we switch to larger source sizes, with the radius of the receiver aperture being increased in the same proportion of source sizes, Gaussian beams continue to exhibit more area scintillations at initial propagation distances, but as the propagation range becomes longer, this situation is reversed, that is, Gaussian beams start to exhibit less area scintillation. This scintillation behavior is inversely proportional to the power captured within the same radius receiver area at small source sizes, while being almost directly proportional at large source sizes.

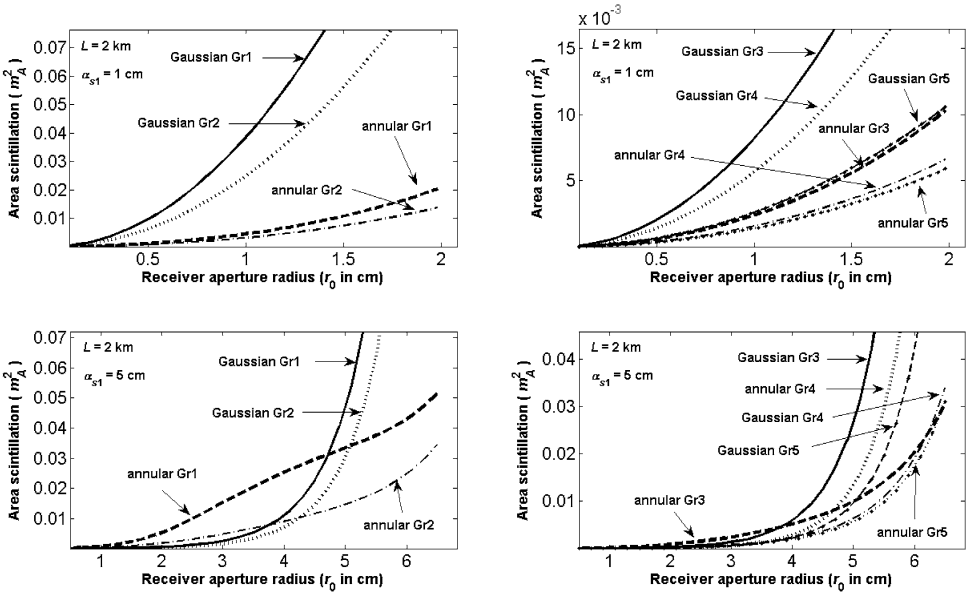

Fig. 8 Variation of area scintillation against receiver aperture radius for Gr1, Gr2, Gr3, Gr4, and Gr5 beams

Wider receiver aperture radius always gives rise to larger area scintillations, but annular beams seem to be more advantageous at smaller source sizes, whereas at large source sizes annular beams have lower scintillations toward larger receiver aperture sizes.

Acknowledgement I am grateful to Emre Sermutlu, member of academic staff in Computer and Mathematics Department of Çankaya University for provision of the quadruple integral routine, which was used in solving (7) numerically.

References

1. V.I. Tatarski, *Wave Propagation in a Turbulent Medium* (McGraw–Hill, New York, 1961)
2. A. Ishimaru, *Wave Propagation and Scattering in Random Media*, vol. 2 (Academic Press, New York, 1978)
3. L.C. Andrews, R.L. Phillips, *Laser Beam Propagation Through Random Media* (SPIE, Bellingham, 2005)
4. Y. Baykal, H.T. Eyyuboğlu, Appl. Opt. **45**, 3793 (2006)
5. H.T. Eyyuboğlu, Y. Baykal, J. Opt. Soc. Am. A **24**, 156 (2007)
6. H.T. Eyyuboğlu, Y. Baykal, Appl. Opt. **46**, 1099 (2007)
7. Y. Baykal, H.T. Eyyuboğlu, Appl. Opt. **46**, 5044 (2007)
8. Y. Baykal, H.T. Eyyuboğlu, Y. Cai, Proc. SPIE **6936**, 69360B–1 (2008)
9. Y. Cai, Y. Chen, H.T. Eyyuboğlu, Y. Baykal, Opt. Lett. **32**, 2405 (2007)
10. S.A. Arpali, H.T. Eyyuboğlu, Y. Baykal, J. Mod. Opt. **55**, 227 (2008)
11. Y. Chen, Y. Cai, H.T. Eyyuboğlu, Y. Baykal, Appl. Phys. B **90**, 87 (2008)
12. H.T. Eyyuboğlu, Y. Baykal, Y. Cai, Appl. Phys. B **91**, 265 (2008)
13. H.T. Eyyuboğlu, Y. Baykal, E. Sermutlu, Y. Cai, Appl. Phys. B **92**, 229 (2008)
14. Y. Cai, H.T. Eyyuboğlu, Y. Baykal, J. Opt. Soc. Am. A **25**, 1497 (2008)
15. H.T. Eyyuboğlu, E. Sermutlu, Y. Baykal, Y. Cai, O. Korotkova, Appl. Phys. B **93**, 605 (2008)
16. H.T. Eyyuboğlu, Y. Baykal, E. Sermutlu, Y. Cai, O. Korotkova, J. Opt. Soc. Am. A **26**, 387 (2009)
17. Y. Baykal, H.T. Eyyuboğlu, Y. Cai, Appl. Opt. **48**, 1943 (2009)
18. Ç. Arpali, C. Yazıcıoğlu, H.T. Eyyuboğlu, S.A. Arpali, Y. Baykal, Opt. Express **14**, 8918 (2006)
19. H.T. Eyyuboğlu, Appl. Phys. B **88**, 259 (2007)